

Exploitation of an oil field using AVO and post-stack rock property analysis methods

Andrew J. Royle

ABSTRACT

Prospecting for new reservoir zones in mature trends often requires new exploration tools. The Colony sand member in east-central Alberta and Saskatchewan has been heavily explored using conventional seismic techniques to map subsurface geology and structure. The main diagnostic tool used to delineate the channel sand trends of the Colony sand member has been identification of “bright spot” anomalies. A relatively small amount of AVO/LMR™ work has been done on the Colony sand member. This is due to a combination of factors, including the high success rate using conventional techniques, and the fact that AVO/LMR™ techniques generally are not as effective at highlighting oil zones such as the Colony sand member compared with gas zones. Our goal was to see if AVO/LMR™ techniques would complement the drilled locations and possibly identify new drilling targets. AVO and LMR™ methods were successfully applied to a 3-D dataset to further delineate Colony channel reservoirs.

INTRODUCTION

The Colony sand member is the uppermost unit of the nine member informal subdivision of the Manville Group, and consists of shales, siltstones, coals, and sandstones. The term Colony member sandstone has a strong genetic connotation as it is commonly associated with thick shoestring channel sandstones which trend south to north and northwest throughout much of east-central Alberta and Saskatchewan (Putnam and Oliver, 1980). Wrightman et al. (1981) illustrated that the reservoir sandstones of the Colony member are made up of several stacked paleochannel deposits. Their work also suggested an eastern basin configuration for the upper Manville and paleodrainage also in that direction. Putnam and Oliver (1980) defined the depositional environment for the upper Mannville sub-group as an extensive complex of anastomosing channel sandstones encased within siltstones, shales, coals, and thin sheet sandstones; this is capped by the marine shales of the Joli Fou formation. Three distinct facies units (Figure 1) are associated with this model. They include (A) channel facies, (B) crevasse splay facies, and (C) interchannel wetland facies.

A small 3-D approximately one section in size is used in this analysis along with available well data. The 3-D survey includes 131 inlines and 101 crosslines with a bin size of 25 by 25 metres. Nine wells are present on the 3-D but only 3 contain sufficient well curves (sonic and density) for inversion. Unfortunately no shear wave sonic data was available in the area so the shear wave logs were estimated using relationships with SP logs. Most of these wells were drilled on “bright spot” anomalies but not all of them were targeted on the Colony sand. Figure 2 shows a map of the 3-D displaying the dimensions of the survey and the well locations. Wells 13-13, 10-14, and 16-14 are noted because they contain sonic and density curves and

will be used throughout this paper for well modelling and inversion. They were also used in the building of the velocity model for ray-tracing.

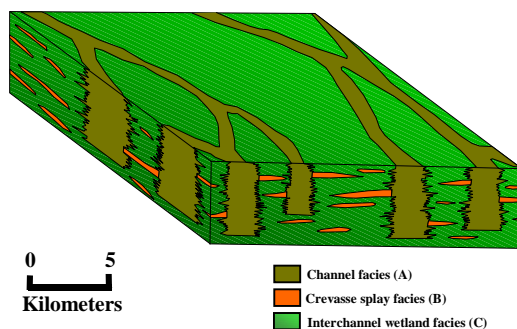


FIG. 1. Depositional model for upper Mannville sub-group (after and Oliver, 1980).

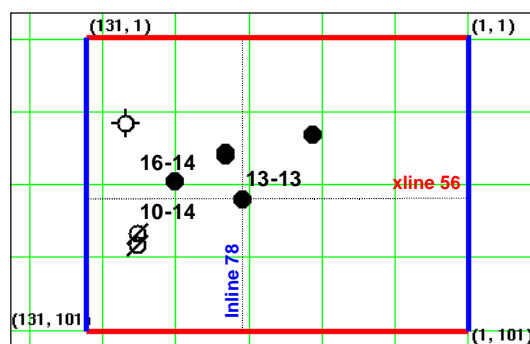


FIG. 2. 3-D base map showing well and seismic lines displayed in this paper.

TECHNIQUES

Several techniques were used in an attempt to extract pore fluid and lithology information from the seismic and well log data. These techniques will be described briefly in the following section.

AVO or Amplitude Variation with Offset searches for a variation in the amplitude of a seismic reflection with offset on an NMO corrected CMP gather. The use of AVO as a direct hydrocarbon indicator in clastic rocks is based on changes to the P-wave velocity (V_P) to S-wave velocity (V_S) ratio of a reservoir rock when gas is introduced into pore spaces (Allen and Peddy, 1993). P-waves are sensitive to changes in pore fluid; the introduction of gas into the pore spaces of a rock greatly reduces the P-wave velocity. The pore space constituent on the other hand does not affect the velocity of S-waves. The change in the ratio of P-wave velocity to S-wave velocity (characterized by Poisson's Ratio) causes the "partitioning" of an incident wave (i.e., into its P-wave and S-wave reflected and refracted components) to differ for the case of a gas-sand/shale or gas-sand/wet-sand reflector from that of most other reflectors. The reflections associated with some reservoirs for gas bearing rocks increase in amplitude with offset relative to other reflectors. This increase in amplitude is rare on seismic data; the majority of reflections decrease in amplitude

with offset. Therefore, AVO analysis is a search for an anomalous seismic response (Allen and Peddy, 1993).

Lambda-Mu-Rho Analysis (LMR™) aims to extract lithology and pore fluid information from seismic and well log data. The conversion of velocity measurements to Lamé's moduli parameters of rigidity (μ) and "incompressibility" (λ) offers new understanding into the original rock properties (Goodway et al., 1997). The Lamé parameters μ , λ , and ρ , which represent "incompressibility", rigidity, and density respectively, allow for enhanced identification of reservoir zones. This is due in part to the fact that the compressibility (and hence the incompressibility) of a rock unit is very sensitive to pore fluid content, also to the fact that lithologic variations tend to be better characterized by fundamental changes in rigidity, "incompressibility", and density as opposed to changes in V_P and V_S . In short, the power of the method stems from the fact that these moduli relate directly to the porosity and lithology attributes of sedimentary rocks. Figure 3a shows a rock matrix that is unstressed; here the rock will have the maximum amount of pore space between its grains.

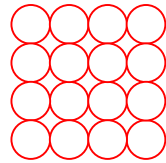


FIG. 3a. Unstressed rock matrix

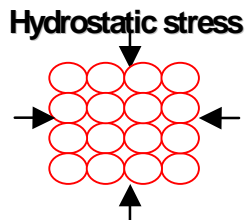


FIG. 3b. Compressed rock matrix

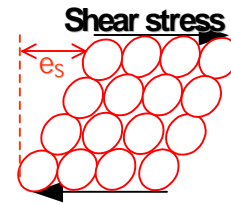


FIG. 3c. Sheared rock matrix

When compression (hydrostatic stress) is applied to a rock (Figure 3b), the compression squeezes the grains causing a decrease in the pore space. If fluids such as oil or water are introduced to the pore space, they will resist the compression by increasing the pressure against the grains and produce a more incompressible rock. The introduction of gas into the pore space will give low incompressibility. This is because gas cannot resist the compression as effectively as the oil or water. Carbonates and igneous rocks have a harder framework and therefore they will have high incompressibility values regardless of pore fluid content. Figure 3c shows a sheared rock matrix, where shearing (shear stress) attempts to slide grains across each other. The pore space volume remains essentially unchanged during the process of shearing regardless of pore fluid type; therefore rigidity, which measures a rock resistance to shearing, should characterize lithology as opposed to pore fluid. Shales are more susceptible to shearing than sands, because of the nature of their grain orientation, giving them low rigidity values. Carbonates due to their rigid framework resist shearing and therefore have high rigidity values. $\lambda\rho^{\text{TM}}$ and $\mu\rho$ volumes can be considered independent and interpreted separately. Lithologies tend to separate along "orthogonal boundaries" in a crossplot of $\lambda\rho^{\text{TM}}$ versus $\mu\rho$.

INTERPRETATION AND RESULTS

Prior to the interpretation of the key horizons the 3 wells containing the sonic and density logs were tied to the seismic. This aided in determining the location of the key seismic markers on the 3-D volume. Figure 4 shows the well ties for wells 13-13 and 10-14.

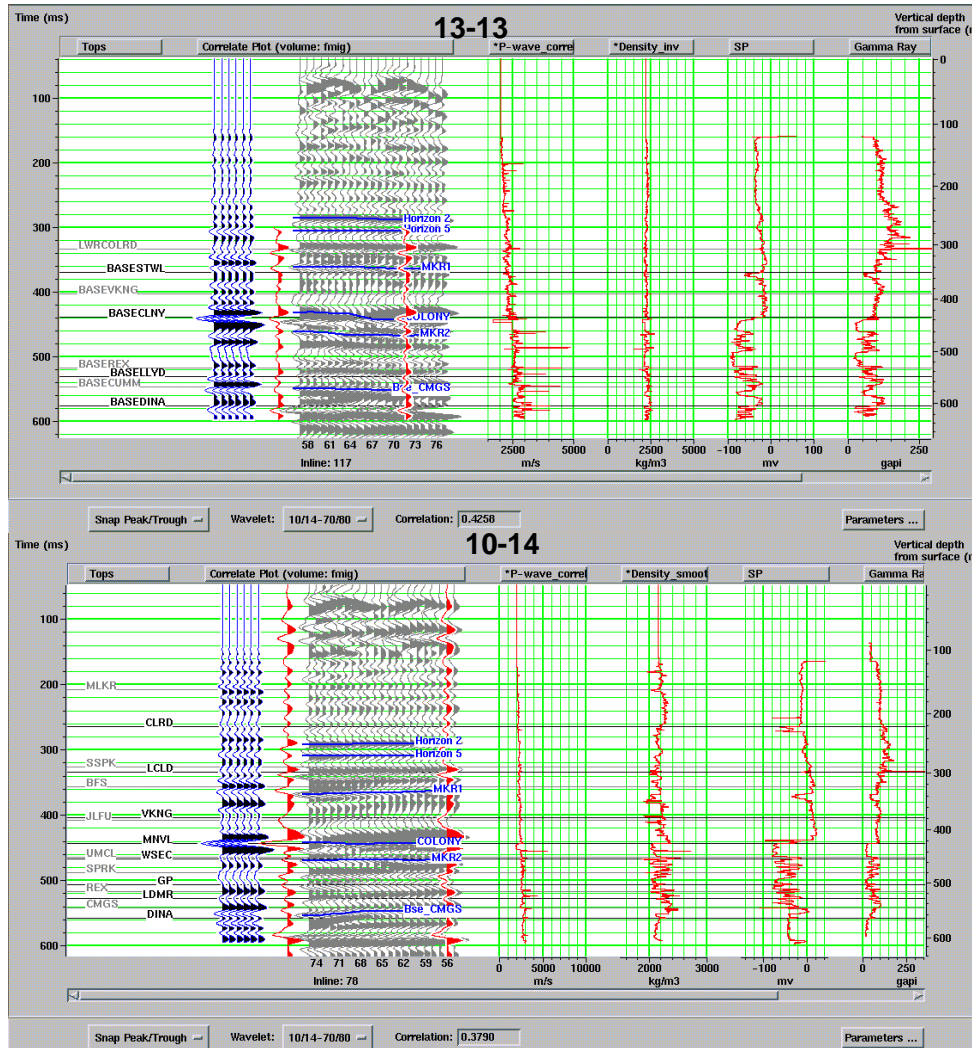


FIG. 4. Well tie displays for wells 13-13 and 10-14.

After the locations of the key horizons were determined, five key horizons were interpreted on this 3-D data set, three of which were used to create a detailed velocity model and to constrain the inversion model. The main horizons include the Colony channel sand and the Waseca sand which lies just beneath the Colony sandstone member. The Colony sand horizon pick is a complicated horizon to interpret especially off the channel. A strong trough classifies the colony channel pick but off the channel it can be represented by a peak or a weak trough. Figure 5 shows inline 78 and crossline 56 from the 3-D volume that intersects at Well A, the “bright spots” can be seen at the Colony channel level. The time-structure map (Figure 6) for the

Colony shows a northeast-southwest trend but the colony amplitude map (Figure 7) clearly delineates the Colony channel extents in this region. The channel extents are drawn on the amplitude map; this demonstrates the channel facies (A) of the depositional model (see Figure 1). Two channels can be clearly seen trending northeast southwest and possibly merging in the southwest. A possibility of crevasse splay deposits (facies B) was interpreted from this amplitude map. Two wells are located on this structure in the middle of the 3-D possibly drilled on this feature.

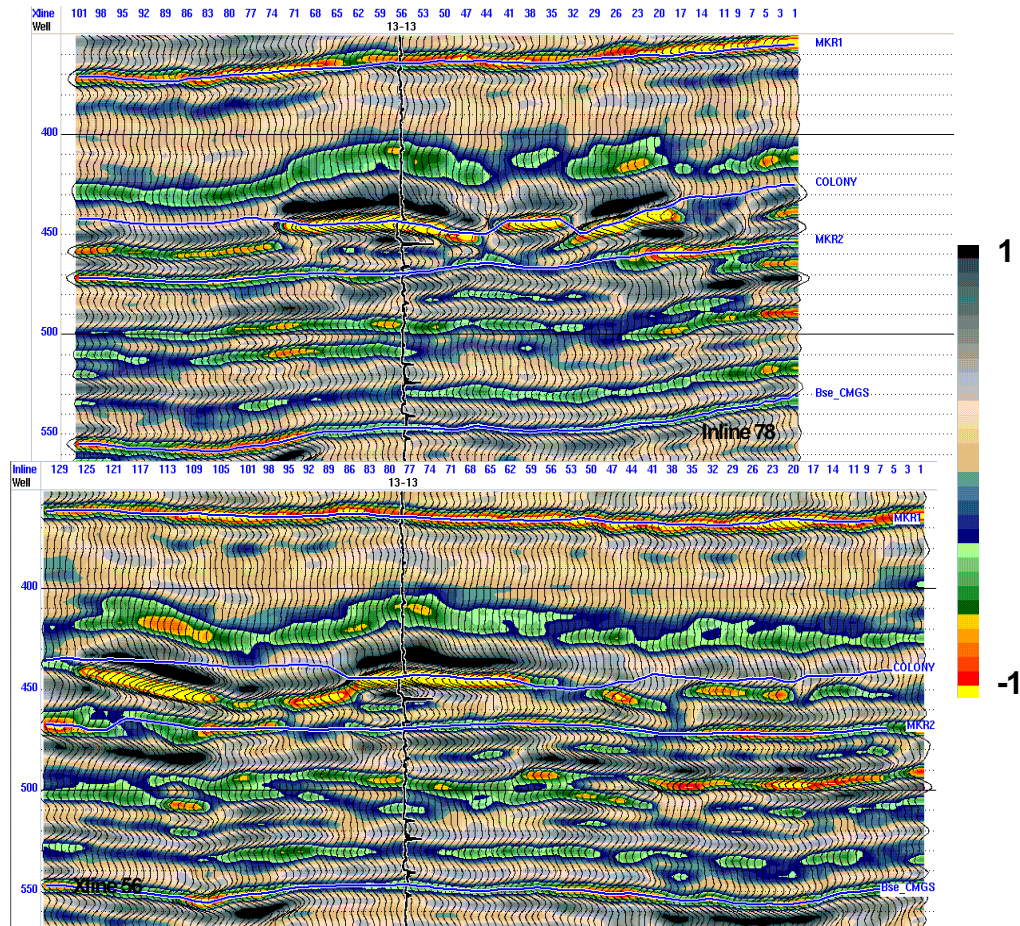


FIG. 5. Inline 78 and crossline 56 from the 3-D, that intersect at well A.

Walker and James (1992) stated that anastomosing channels consist of several active channels of low to high sinuosity and it is within this system that crevasing is encouraged when channels are plugged with bedload deposits. A second derivative volume was created on the seismic volume with the goal of better delineating the channel. A time slice from the second derivative volume at the Colony level is displayed in Figure 8; the dimensions of the channels again can be clearly identified.

Once the dimensions of the channel were identified, AVO/LMR™ techniques were applied to further constrain the drilling targets on the 3-D volume. AVO forward modelling was performed in order to determine if an AVO anomaly should be expected. Two of the wells on the 3-D were modeled in an attempt to predict the

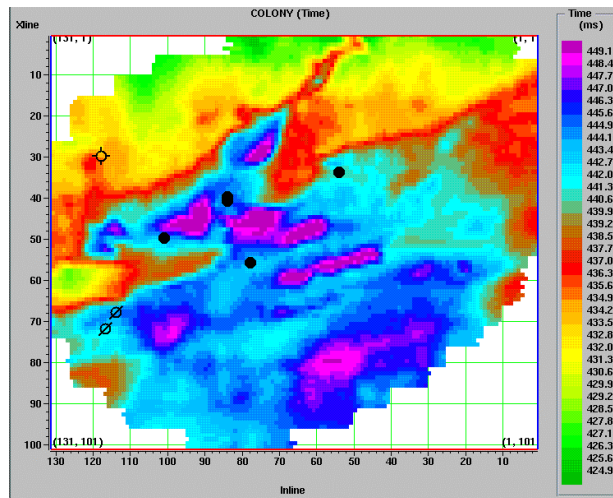


FIG. 6. Colony time-structure map.

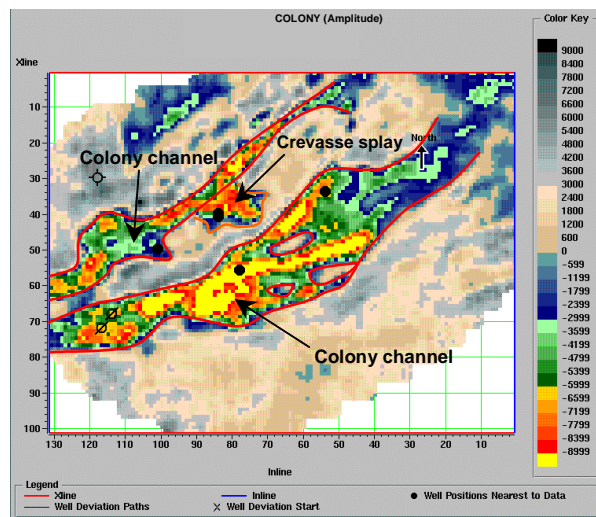


FIG. 7. Colony amplitude map.

AVO response for the Colony. The modelling responses from both wells show near identical results. An AVO anomaly was observed at the top (trough) and base (peak) of the Colony. However, the shear wave values were estimated, which may have had an impact on these results. The observed AVO anomaly is not very strong; this may be due to the nature of the hydrocarbon (oil) in the pore spaces. This would be classified as a class 3 AVO anomaly which consists of a “bright spot” anomaly with an increase in amplitude with offset. The results of the AVO well modelling for well B are shown in Figures 9 and 10.

Gradient and intercept volumes were extracted with the intention of extracting pore fluid information. Gradient (G) and intercept (I) volumes were computed at each time sample at each CMP location by performing a least squares fit of Shuey’s equation ($amp = I + G \sin \theta$, where θ is incident angle) to the observed data. The gradient volume shows the rate of change of the amplitudes with incident angle, while the intercept volume shows the zero-offset response and should emphasize a “bright

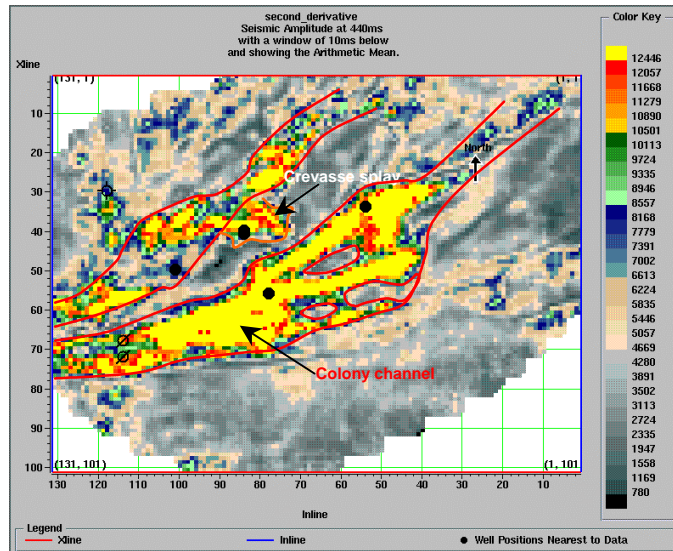


FIG. 8. Second derivative map at Colony level.

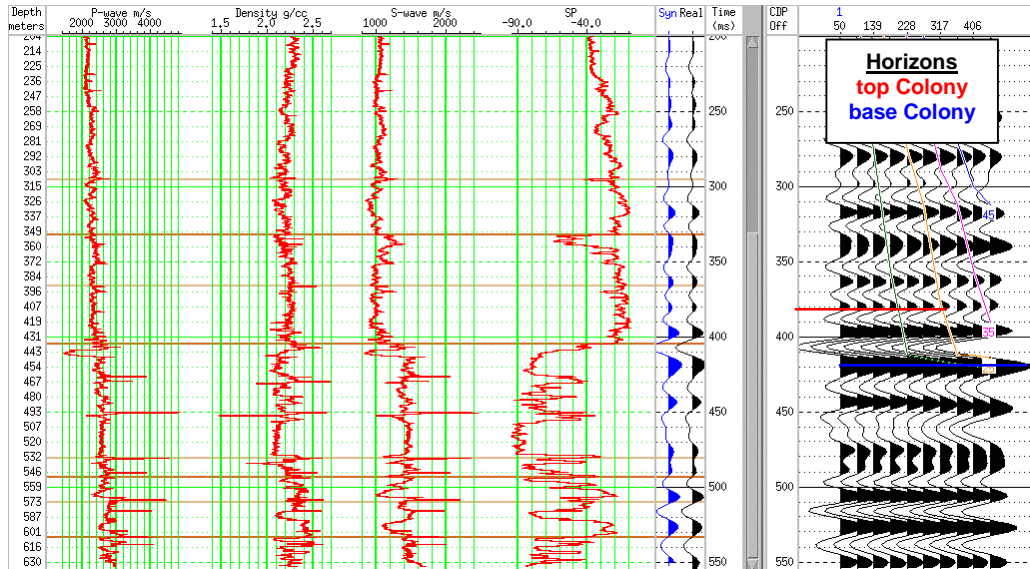


FIG. 9. AVO modelling at 11/10-14.

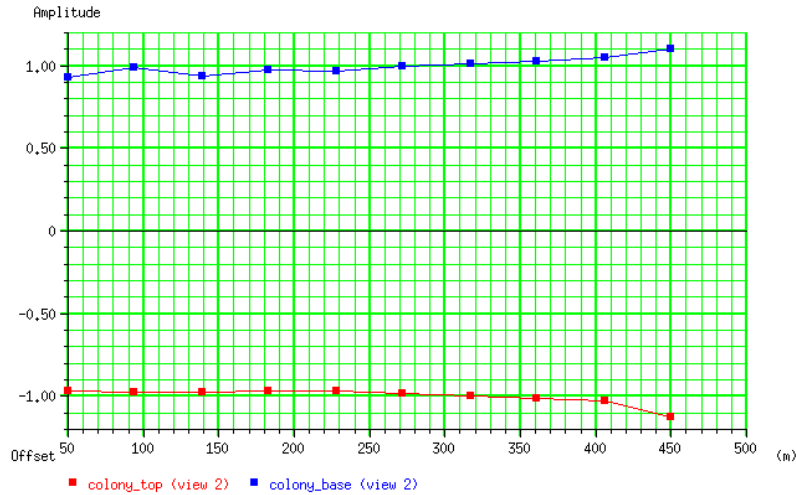


FIG. 10. Amplitude vs. offset plot for Colony horizon picks.

spot” anomaly. These volumes are usually multiplied giving a product volume; this is done to enhance class 3 or “bright spot” AVO anomalies. The product volumes for inline 78 and crossline 56 are shown on Figure 11.

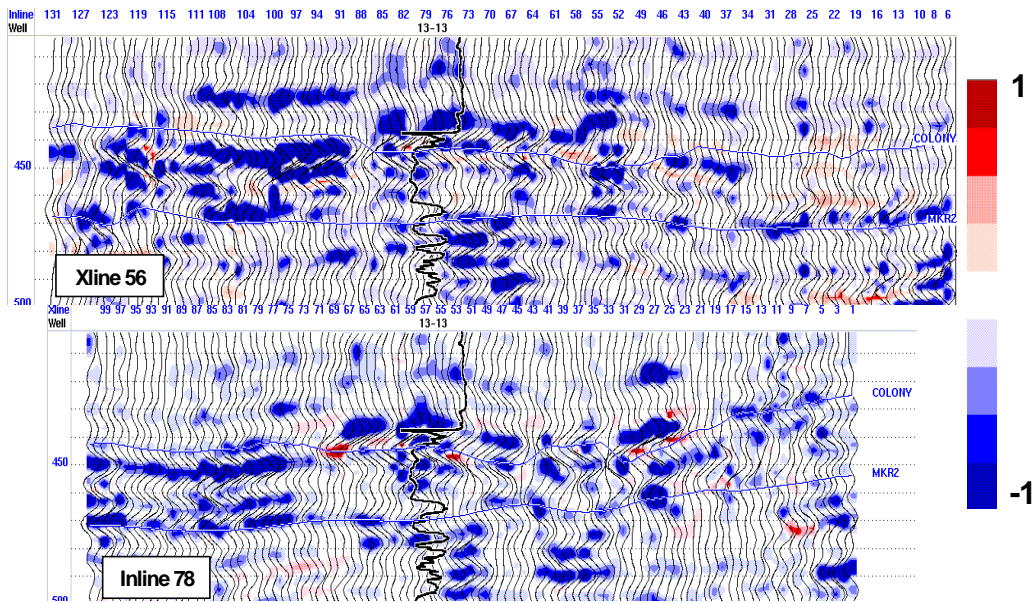


FIG. 11. Product (intercept*gradient) volumes at inline 78 and crossline 56.

A weak AVO response can be seen at the Colony level on these stacks similar to what was expected after modelling. A red colour on this section indicates an increase of amplitude with offset while blue denotes the opposite. A time slice of the product volume was generated (Figure 12) at the Colony level. AVO anomalies can be seen at certain well locations on the 3-D.

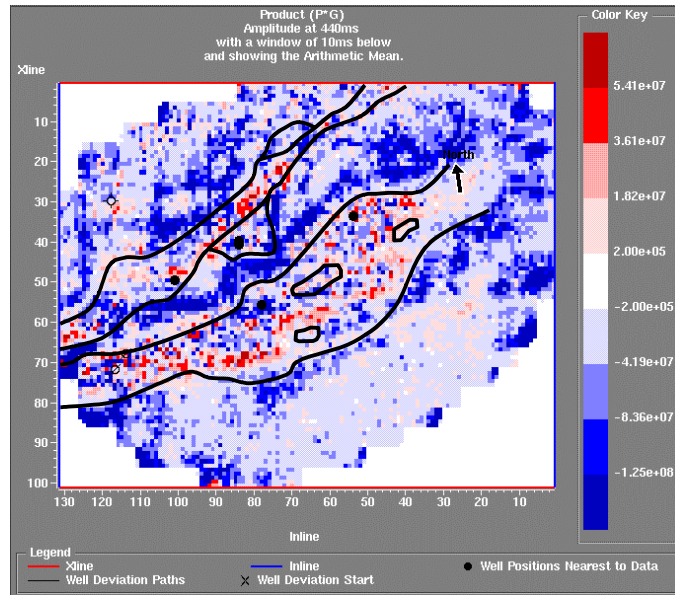


FIG.12. Time slice of the product volume at the Colony level.

Crossplotting allows us to inspect two volumes at once, highlight anomalous zones and display them on a stacked section. Intercept and gradient volumes are commonly crossplotted; anomalous zones that fall off the background trend should indicate the presence of a hydrocarbon in the pore space of the rock. Figure 13 shows an intercept versus gradient crossplot at inline 78.

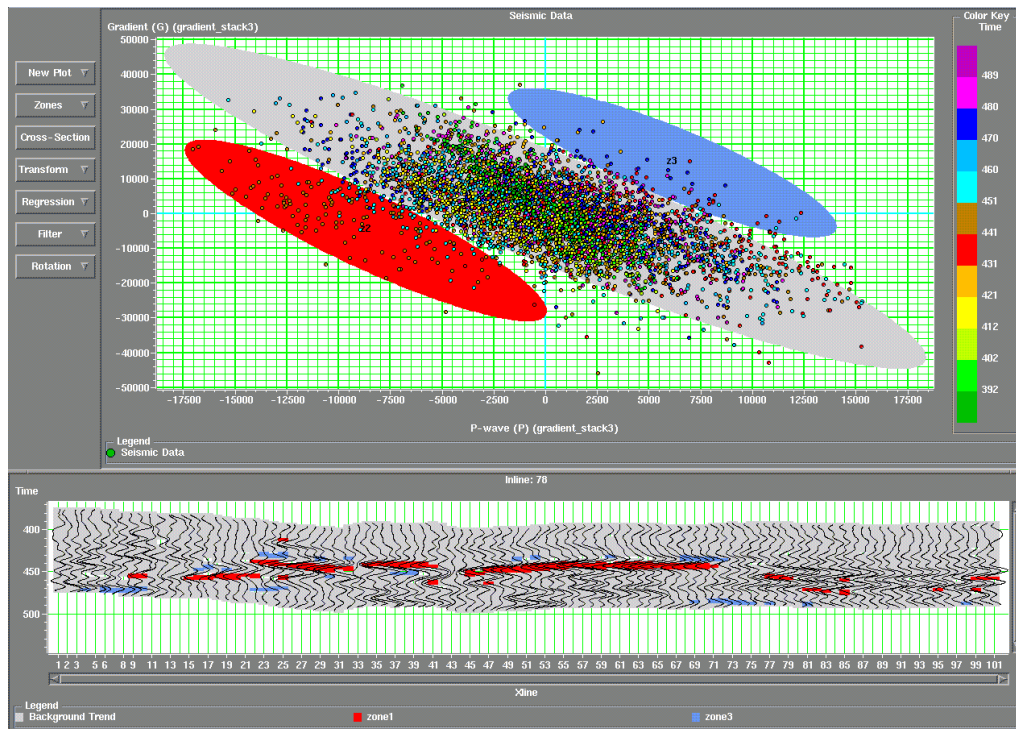


Fig. 13. Intercept vs. gradient crossplot and section at inline 78.

The background trend can be easily identified; the anomalous zones are highlighted and plotted on the stacked section. The highlighted zones from the crossplot were identified for the whole 3-D volume and an anomalous zone volume was compiled. From this volume a time slice was created (Figure 14). This map shows a good fit to the Colony channel and the wells drilled on it (red denotes an increase in amplitude with offset, while blue indicates a decrease).

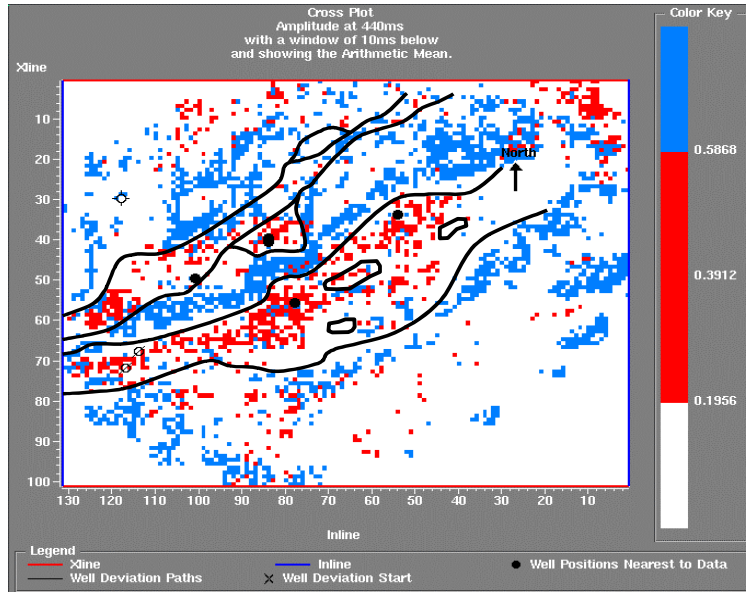


FIG. 14. Time slice of anomalous zones obtained from intercept vs. gradient crossplot.

Encouraged by the positive results obtained with the gradient and intercept volumes, P- and S-reflectivities were extracted in order to attain a Fluid Factor volume. The Fluid Factor numerical quantity is designed to be low amplitude for all reflectors in a clastic sedimentary sequence except for rocks that lie off the “mudrock line”. In the absence of carbonates and igneous rocks, high amplitude reflections on fluid factor traces would be expected to represent gas-saturated sandstones. Essentially this is an attempt to see if the fluid factor will work with oil in the pore space instead of gas. The fluid factor volumes for inline 78 and crossline 56 are shown on Figure 15.

A high amplitude response can be seen at the Colony level on these stacks possibly indicating the presence of a hydrocarbon in the pore space of the rock at the Colony level. There is also a high amplitude between 580 and 600 ms-this is the top of the carbonate section and is expected to give a high amplitude response. A time slice of the Fluid Factor volume was generated (Figure 16) at the Colony level.

It can be seen on the time slice that there is a high amplitude response on both channels and not off the channels as expected. These high amplitude zones seem to correspond to the known well locations on the 3-D volume. A crossplot analysis of the P-reflectivity and S-reflectivity volumes was compiled to possibly further isolate the Fluid Factor anomalies. Figure 17 shows a crossplot of P-reflectivity versus S-reflectivity at inline 78.

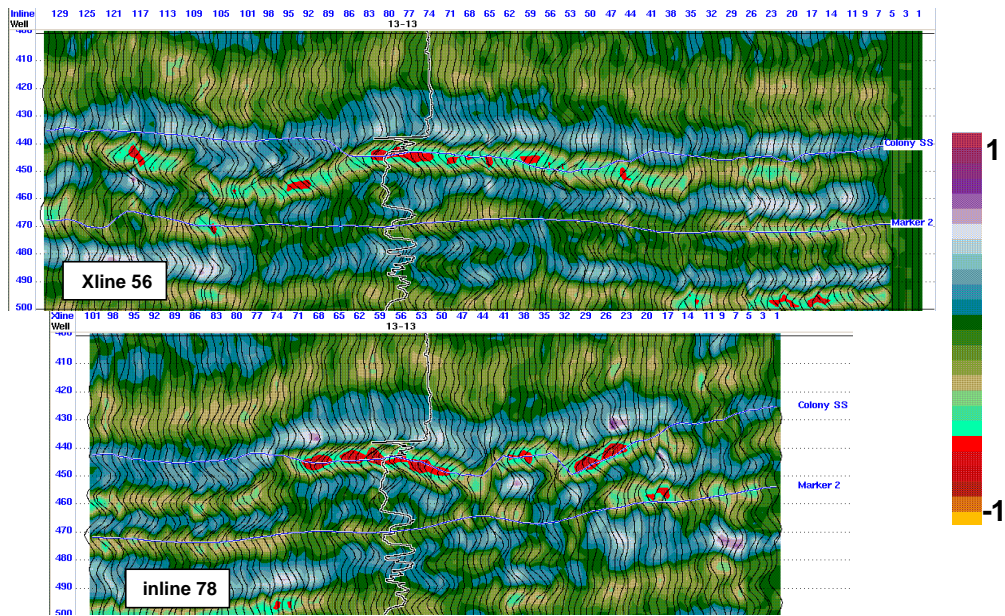


FIG. 15. Fluid Factor volumes at inline 78 and crossline 56 from the 3-D, which intersect at 13-13.

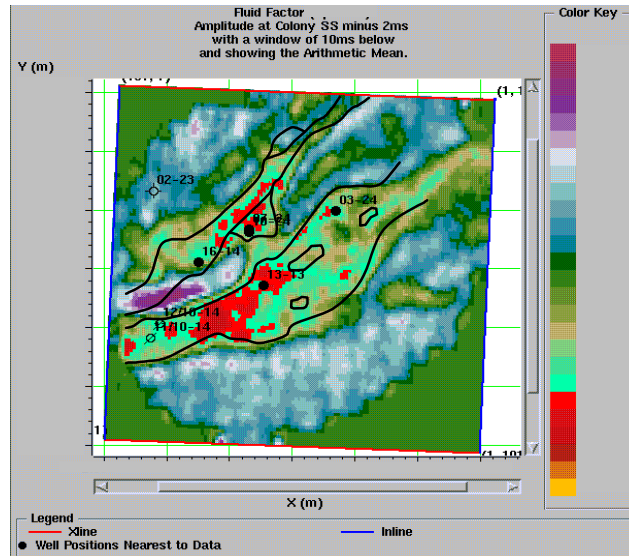


FIG. 16. Time slice of the fluid factor volume at the Colony level.

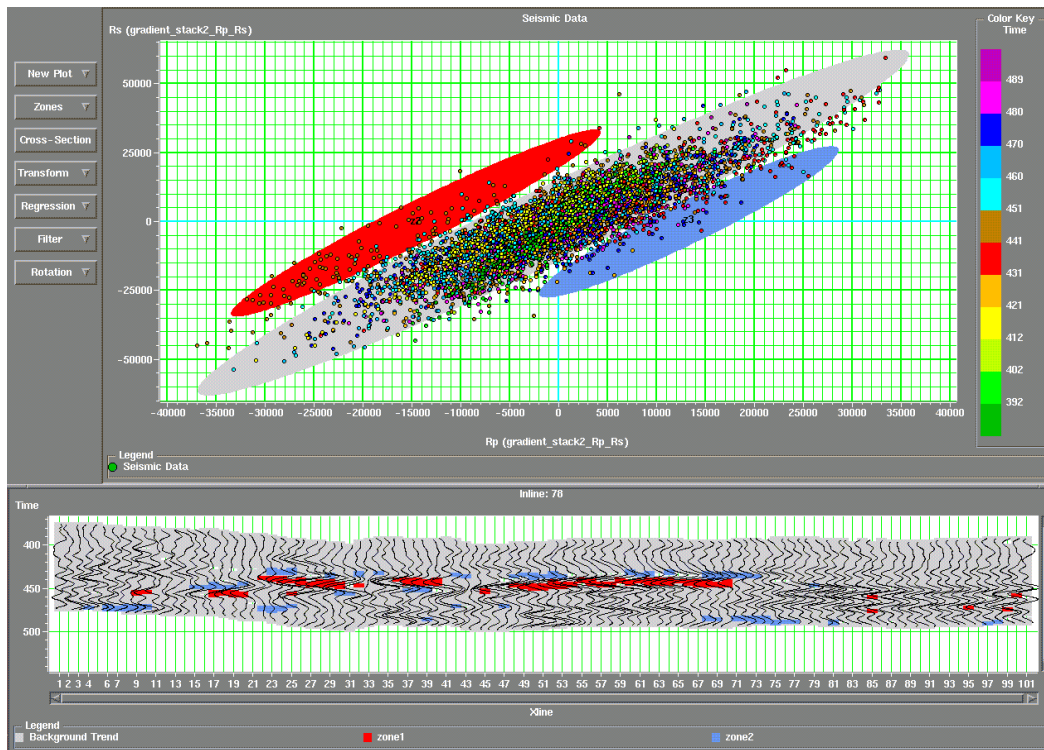


FIG. 17. P-reflectivity vs. S-reflectivity crossplot and section at inline 78.

It can be seen from the crossplot that there are anomalous zones or outliers off the background trend. These outliers were highlighted and displayed on the section. These zones seem to highlight the Colony trough quite distinctly. To get an idea of the distribution of these zones on the 3-D volume a time slice was created at the Colony level (Figure 18).

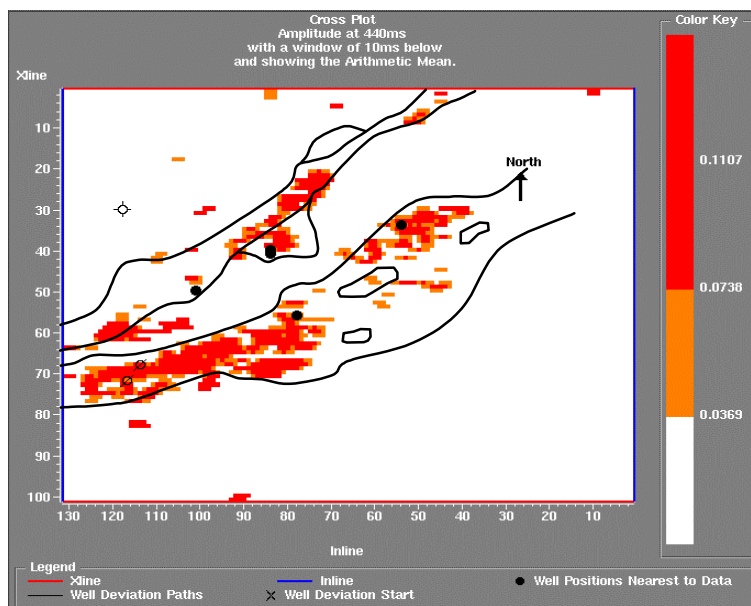


FIG 18. Time slice of anomalous zones obtained from P-reflectivity vs. S-reflectivity crossplot at Colony level.

Several isolated zones are apparent on the time slice and seem to relate to the well locations. The dry hole location in the northwest does not have any anomalies associated with it. The two suspended wells to the southwest on the south channel did have associated oil production before being suspended.

Now that the reflectivity volumes have been produced and assessed, post stack inversion was performed on these volumes with the intent to extract Lamé's parameters lambda (λ), mu (μ), and possibly the bulk modulus (κ). Now we go from interpreting differences across interfaces to differences across intervals. Before inversion was performed, all sonic and density information was correlated to the seismic. The interpreted horizons and the well information constrained P- and S-impedance models which were generated.

Problems were encountered with the S-impedance model. Due to the nature of the pore fluid (oil), a Poisson's ratio of approximately 0.25-0.30 is expected at the Colony sand in this area. With the strong decrease in P-wave velocity in the Colony sand, using the ARCO mudrock (global relationship) equation, shear wave values obtained do not correspond to the expected range of Poisson's ratio and compared to overlying shales. This complicates estimating shear wave values using a global mudrock equation. In order to circumvent this problem, a regional full waveform wave sonic was obtained from the 15-06 well in the region; it is the only shear data available in the area that cuts the Colony zone. This helped predict a regional mudrock trend, which was applied to the well in the survey area. Figure 19 shows the log curves and Figure 20 shows the crossplot between the P-wave and S-wave values at the 15-06 well. It can be seen on the crossplot that there are two distinct zones. The upper zone is linked to the Lower Cretaceous sediments (Colony and below) while the lower zone is linked to the shalier sediment of the Upper Cretaceous. Two mudrock trends were determined from this crossplot; $V_P = 0.542 * V_S - 95.0$ for the upper zone (Lower Cretaceous zone) and $V_P = 0.157 * V_S + 212.2$ for the lower zone (Upper Cretaceous zone). These relationships were applied to the 10-14 and 13-13

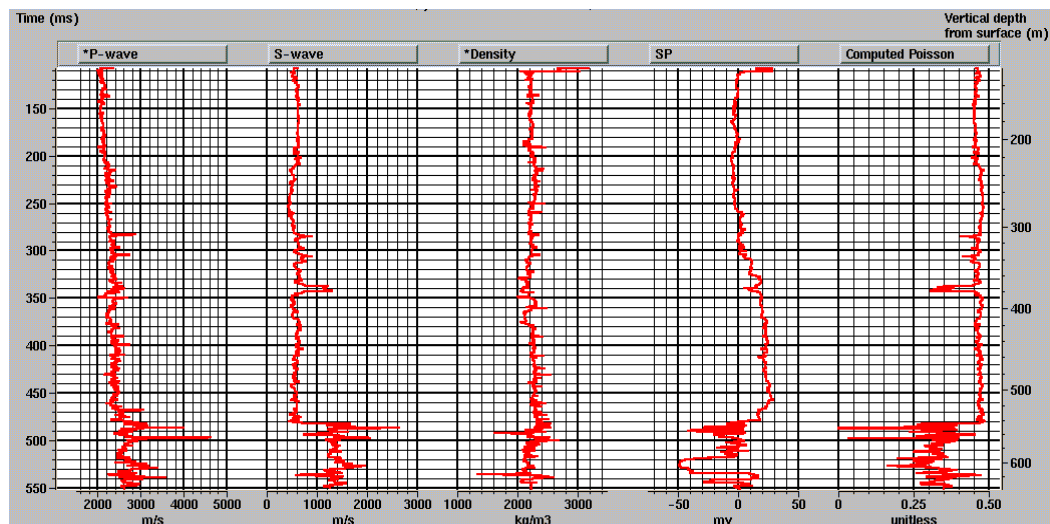


FIG. 19. Log curves at the Pike's Peak 15-06 well.

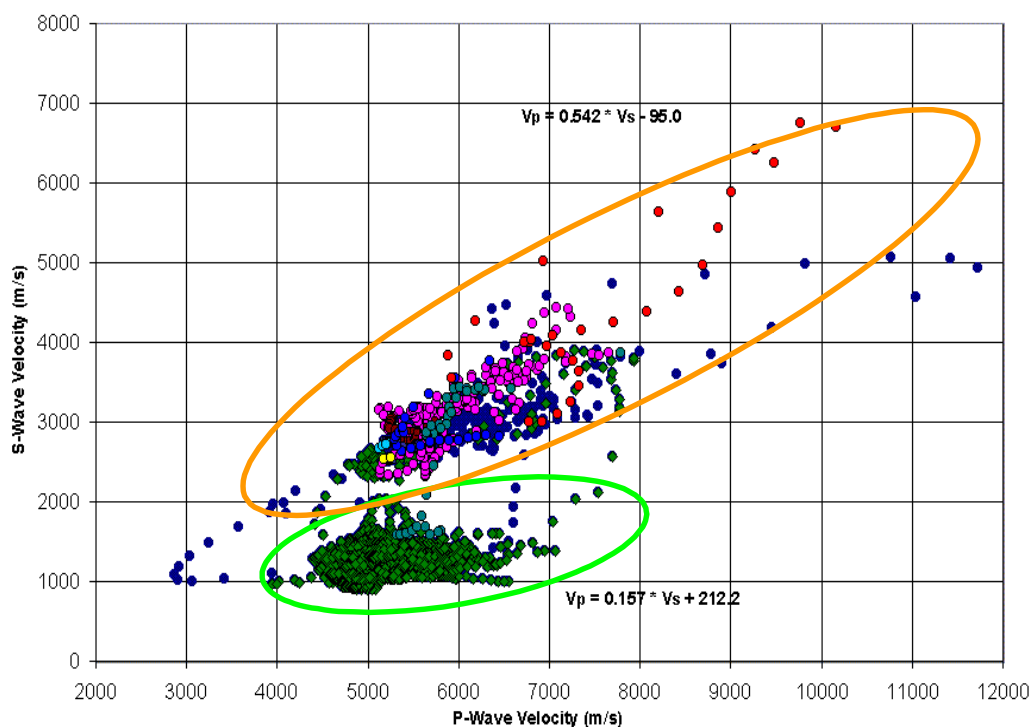


FIG. 20. Crossplot between the *P*-wave and *S*-wave velocity at the regional shear well.

wells prior to the *S*-impedance inversion. The estimated shear wave logs and corresponding Poisson's ratios are quite similar to those of the regional shear well. Once all the log editing was completed, inversion for *P*- and *S*-impedance was performed on the extracted *P*- and *S*-reflectivities. The *P*-impedance sections for inline 78 and crossline 56 are displayed in Figure 21. The impedance ranges from 4000 to 8500 (m/s*g/cc) and there is quite an impedance low at the Colony channel zone. This low could indicate several things such as a porous sand zone, coal, lignite, or shale. We know that this is a porous sand zone but there is a chance that this may be a coal as well. The Colony channels are known to contain coal or shale fill in some areas. There is no way to determine the exact lithology on a *P*-impedance plot, but by comparing it with a *S*-impedance section should correspond to shales or coals; moderate values should represent sandstones, and high determine lithologies can be inferred by elimination. With accurate shear information, a *S*-impedance plot should be able to distinguish between coals-shales, sandstones, and carbonates. This is because since shear waves are unaffected by pore fluid, they should give information about the matrix of the rock. Low values represent carbonates or igneous rock if present. The *S*-impedance sections are displayed in Figure 22 and a fairly sharp impedance contrast can be seen at the Colony horizon. As expected the impedance values to be moderate for a sandstone intervals and low values for the overlying shales. Time slices for both the *P*- and *S*-impedances were compiled and are shown in Figure 23.

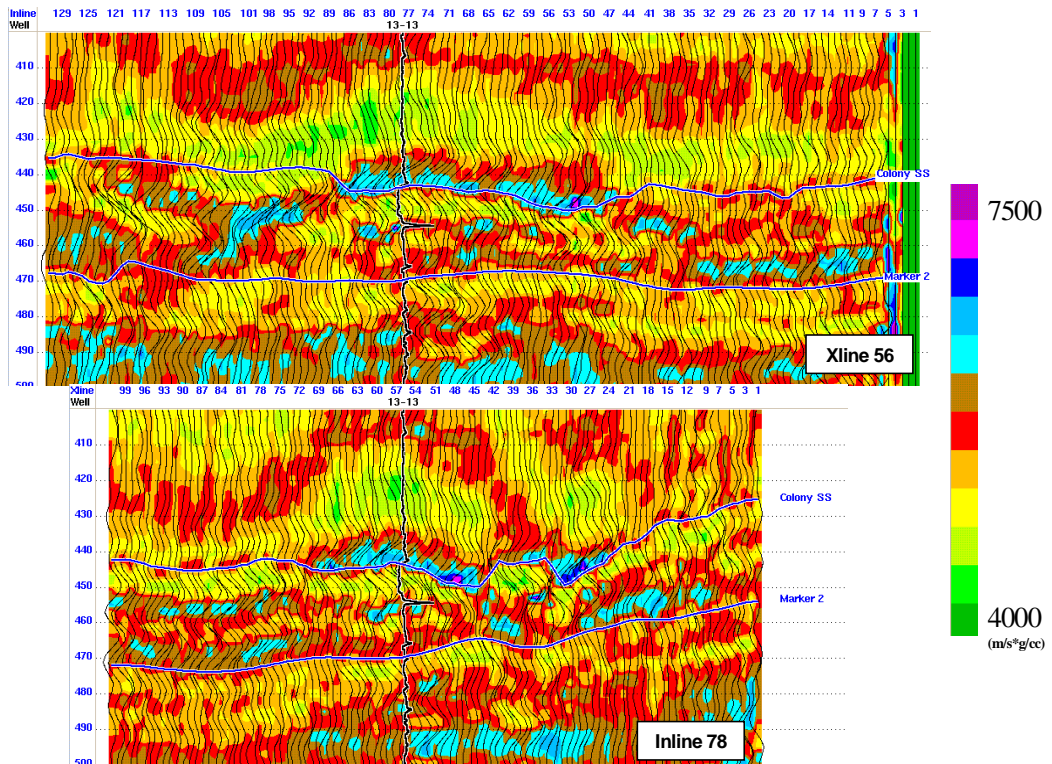


FIG. 21. P-impedance volumes at inline 78 and crossline 56.

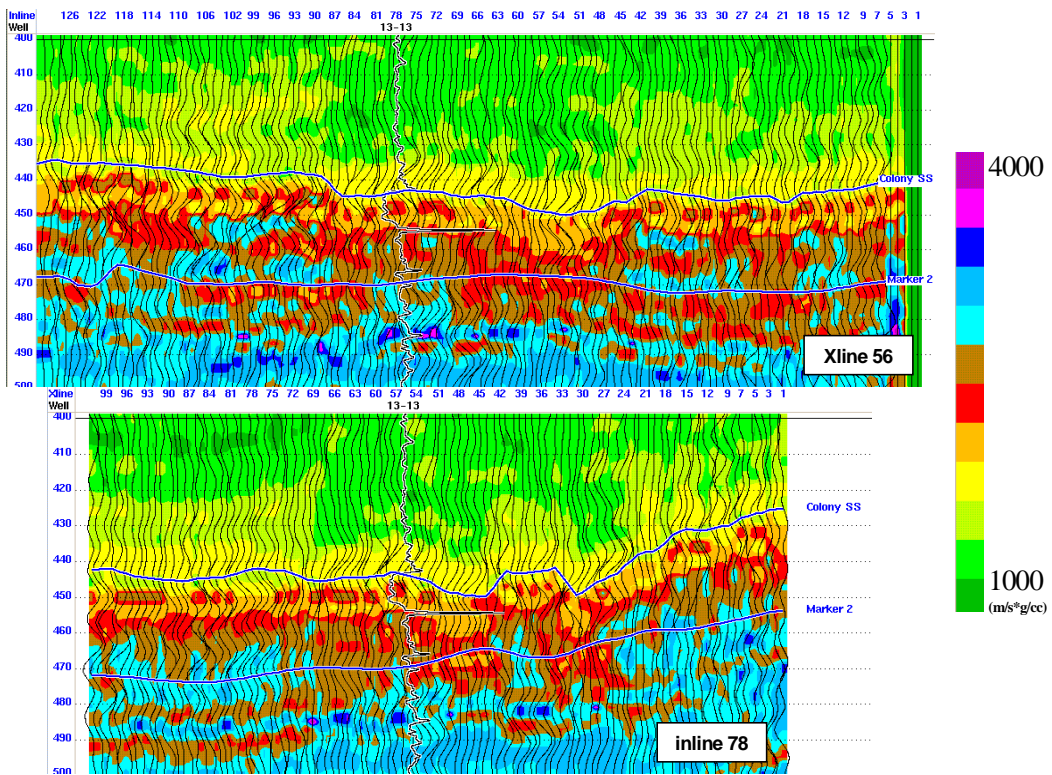


FIG. 22. S-impedance volumes at inline 78 and crossline 56.

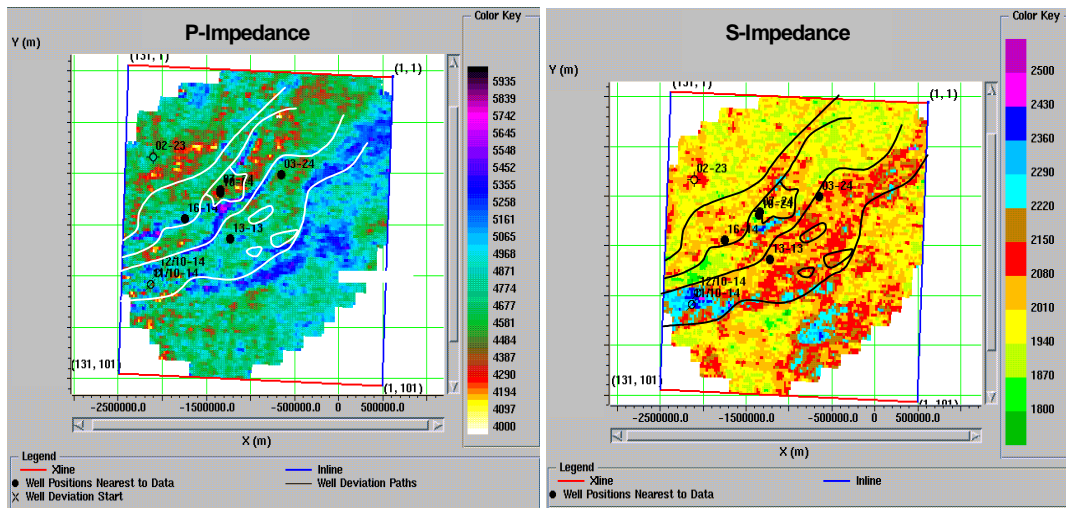


FIG. 23. Time slices of P- and S-impedances at Colony level.

The P-impedance time slice shows good zones of low impedance around some of the producing well locations. Especially at the crevasse splay zone the impedance lows seem to somewhat follow the channel trend. The S-impedance time slice also follows the channel; values on the channel are higher than the values off the channel. As mentioned earlier the sand zones should have moderate to high impedances due to the lack of carbonates at this level. The channel sands seem to have a higher rigidity on the channel than the sediments off the channel.

After P-and S-impedance are attained there is little effort to go the extra step to compute $\Lambda \cdot \rho$ and $\mu \cdot \rho$. The $\Lambda \cdot \rho$ volume was designed to give information about pore fluid and distinguishes between sands, gas sands, shales, coals, and carbonates. The $\mu \cdot \rho$ volume gives information about lithology and distinguishes rock matrix type - sands, shales, coals, and carbonates. The $\mu \cdot \rho$ stack is unaffected by pore fluid and therefore the constituent of the pore space should not affect the values. The $\Lambda \cdot \rho$ sections for inline 78 and crossline 56 are located in Figure 24 and the $\mu \cdot \rho$ sections are located in Figure 25.

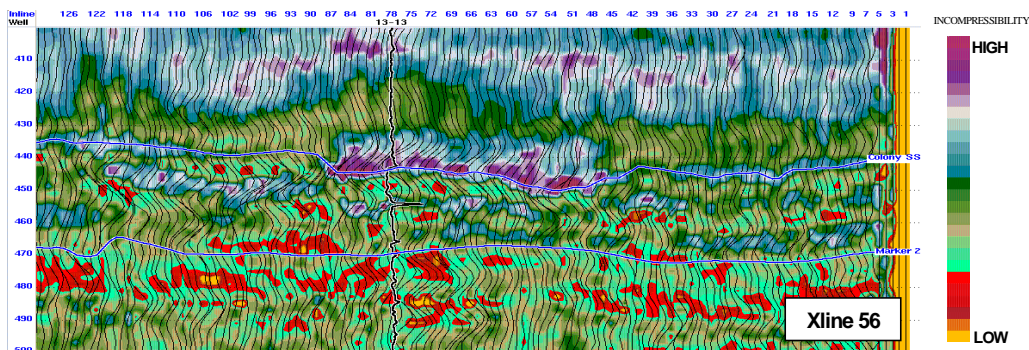


FIG. 24. $\Lambda \cdot \rho$ section at crossline 56.

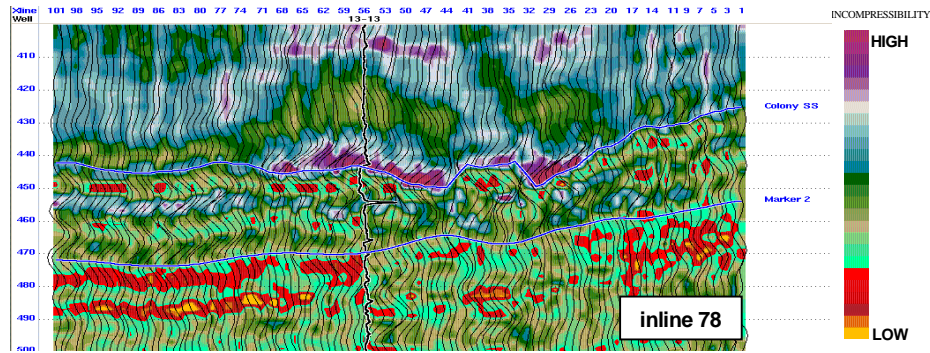


FIG. 24. Lambda*Rho section at inline 78.

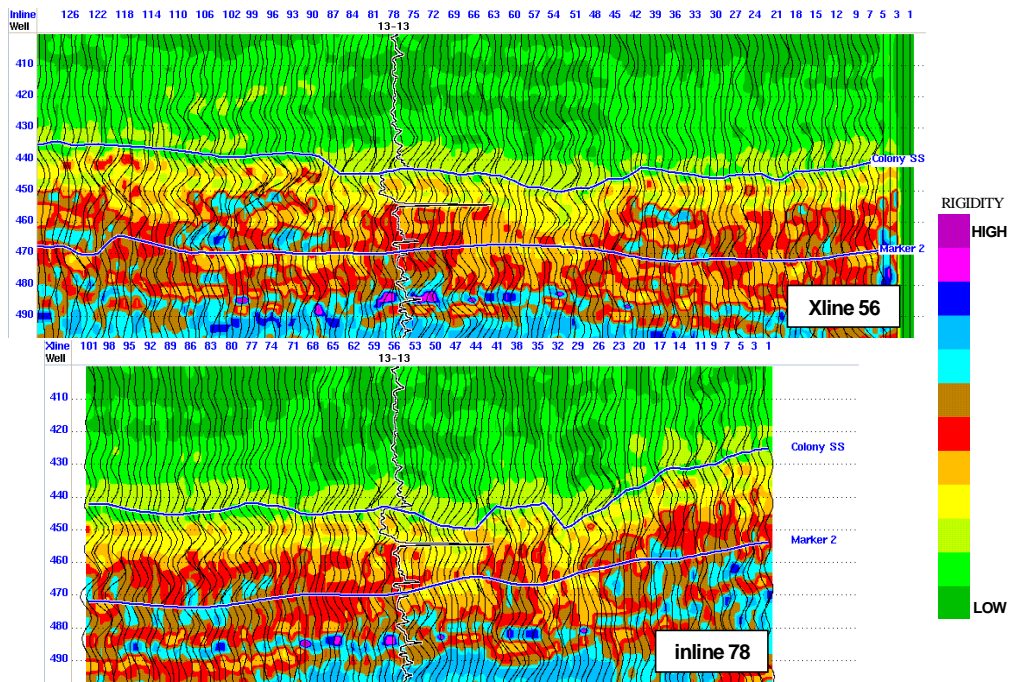


FIG. 25. Mu*Rho sections at inline 78 and crossline 56.

There were expected lows for incompressibility at the Colony horizon on the Lambda*Rho sections compared to the rest of the section. There are also some incompressibility lows of possible interest lower in the sections. The McLaren, Waseca, and other sandstones units are other possible targets in this area. Because of the lack of carbonate rocks in this portion of the data, the incompressibility highs probably correspond to tight sands while the moderate to low values can be shale. The Mu*Rho sections as expected show a moderate rigidity values at the Colony level; this may represent a sand zone. The lowest rigidity values should correspond to coals, then shales, sandstones have moderate values, while carbonates and igneous rocks have the highest values of rigidity. Time slices of the Lambda*Rho and Mu*Rho volumes were generated and are shown in Figure 26.

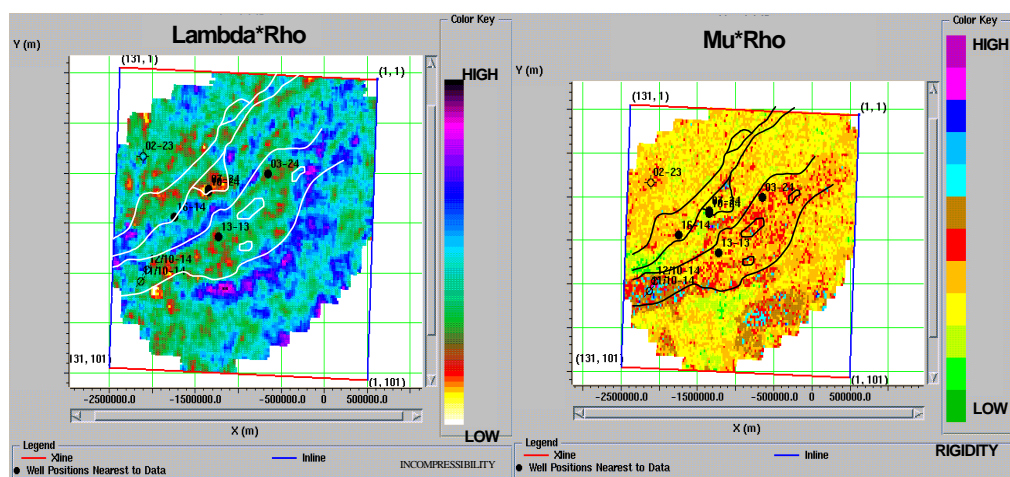


FIG. 26. Lambda*Rho and Mu*Rho time slices at Colony level.

The Lambda*Rho time slice definitely seems to isolate hydrocarbon accumulations at the well locations. The 07-24, 03-24, 13-13, and 10-14 well locations seem to correspond to incompressibility lows. The Mu*Rho time slice shows a good channel sand trend. The channel has higher rigidity values than the surrounding interchannel wetland facies zones (off channel zones) indicating sand quality on the channel zones.

Elastic Impedance Inversion

In a further investigation to extract information on lithology and pore fluid, an elastic impedance inversion was performed on the 3-D volume. Connolly (1999) introduced elastic impedance as a generalization of acoustic impedance for non-normal incidence angle (Whitcombe et al., 2000). An elastic impedance volume is similar to an acoustic impedance volume except that it includes a V_S term in its derivation. This method takes a far angle volume and applies it to a linearized approximation of the Zoeppritz equations (Connolly, 1999) using V_P , V_S , and density log information. Elastic impedance is a function of V_P , V_S , density, and incidence angle. Elastic impedance is generally similar in appearance to acoustic impedance although the absolute numbers are lower; it is a property of elastic impedance that the level decreases with increasing angle (Connolly, 1999).

In preparation for the elastic impedance inversion a 21 to 32 degree and 33 to 44 degree angle volumes were extracted from the dataset. Then elastic impedance logs were created at the 13-13 and 10-14 well locations. A comparison between the acoustic and elastic impedance logs is displayed in Figure 27. It can be seen that the elastic impedance logs show a stronger contrast at the Colony zone than the acoustic impedance logs. These logs formed the input model for the elastic impedance inversion. Time slices at the Colony level were compiled to show the 3-D distribution of the elastic impedance lows. The time slice for the 21 to 32 degree elastic impedance volume is displayed in Figure 28 and the 33 to 44 degree elastic impedance volume in Figure 29. As seen on the logs there is an elastic impedance low at the Colony zone possibly indicating a hydrocarbon accumulation. The 21 to 32

degree elastic impedance time slice shows impedance lows at several of the well locations (03-24, 07-24, 10-14, and 02-23). However there is a low at the 02-23 dry hole location; this may possibly be due to a lithologic variation such as shale or coal. This well log suite was not included in this analysis and therefore the nature of the lithology is not known at this location. The 33 to 44 degree elastic impedance time slice also shows lows at several of the well locations (03-24, 07-24, 10-14, and 13-13). The 33 to 44 degree elastic impedance volume shows good correlation with the well control on the 3-D survey. There is no anomaly at the 02-24 well location and there is an anomaly at the 13-13 oil well location. This shows similar results to the fluid factor crossplot constrained and LMR™ results but seems to be even more constrained.

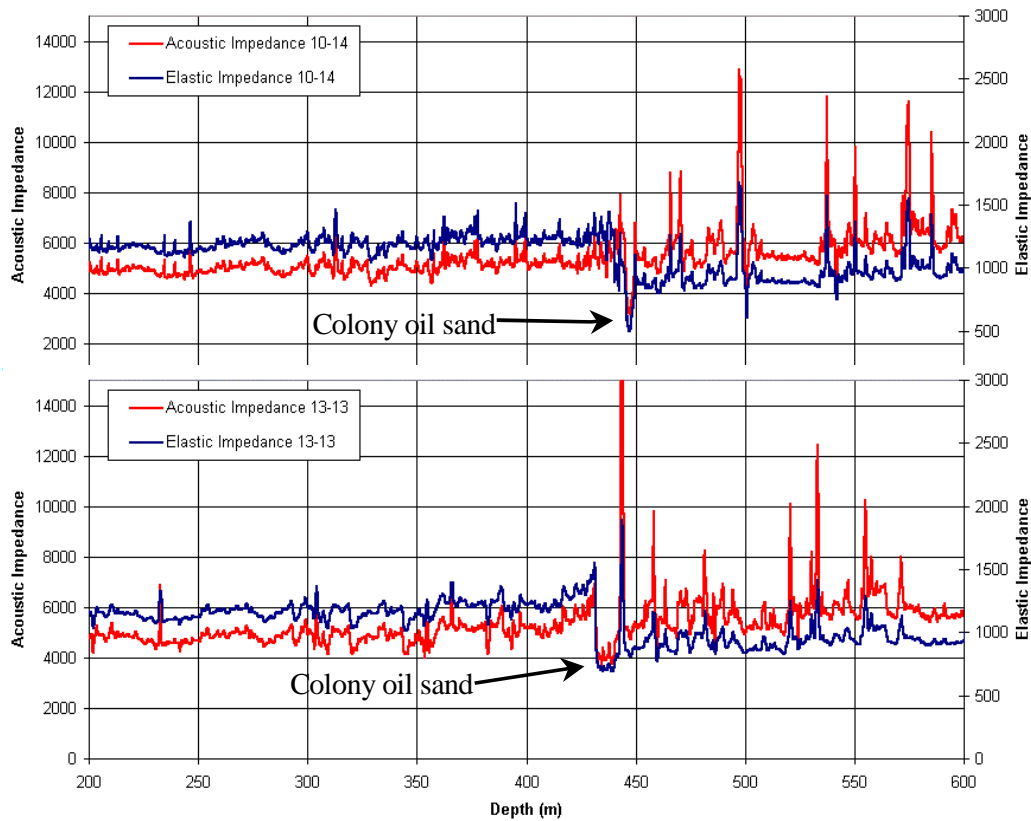


FIG. 27. Comparison between the acoustic and elastic impedance logs.

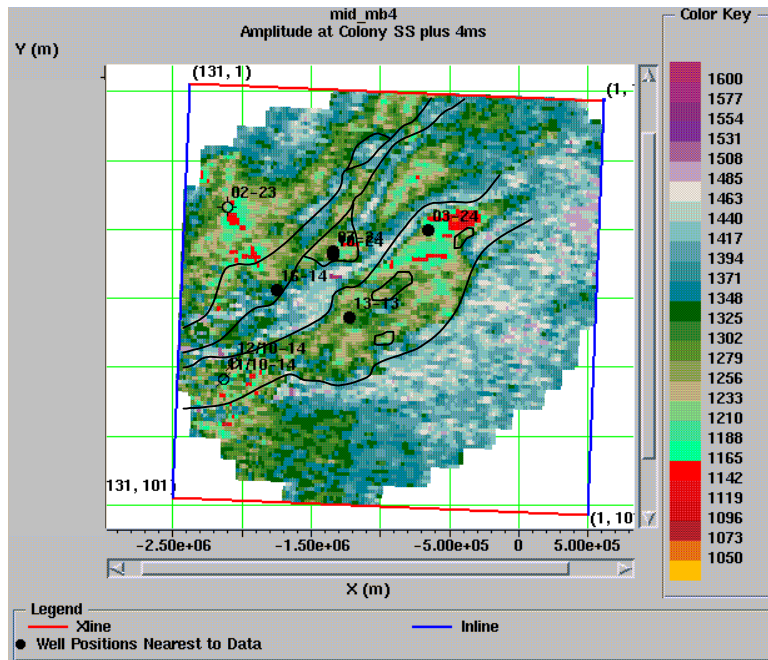


FIG. 28. 21 to 32 degree elastic impedance time slice at Colony.

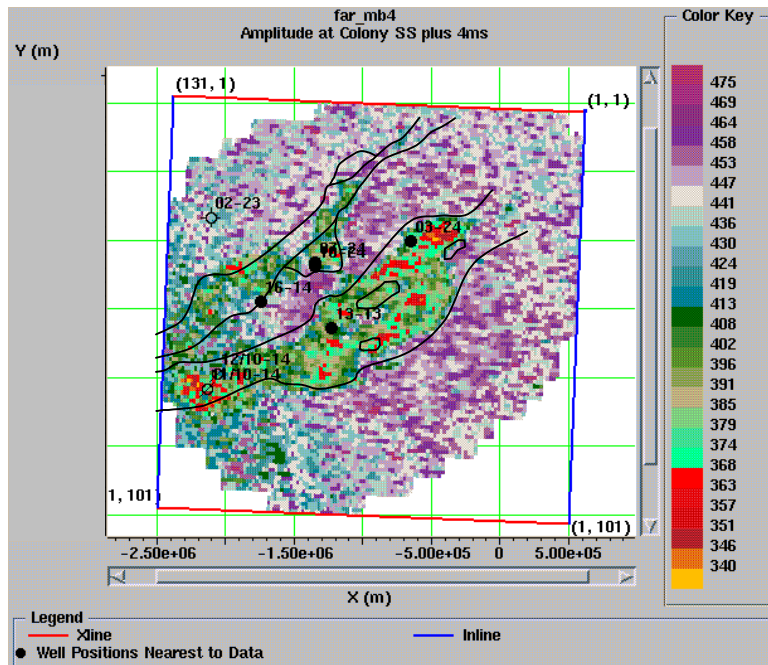


FIG. 29. 33 to 44 degree elastic impedance time slice at Colony.

CONCLUSIONS

The channel is delineated quite well from the Colony amplitude map and it can be seen that the existing wells were drilled on structurally high “bright spots”. Using AVO analysis my goal was to further delineate the Colony pool reservoirs. The AVO modelling showed positive results heading into AVO analysis. Using AVO modelling a class III AVO anomaly was detected. The gradient and intercept analysis did a reasonable job and the anomalies did trend within the channel zones. The anomalies did account for the producing oil wells on the 3-D and the one dry hole on the 3-D was off the anomalies. The Fluid Factor analysis also seemed to show an anomalous trend that fell within the channel boundaries. Crossplotting the P- and S-reflectivities proved to be a great attribute to isolate the separate oil pools on the 3-D volume. The only question that came from the AVO analysis was “why wasn’t there any response from the base of the reservoir zone?” (analysis concentrated on Colony trough) This could possibly be due to the thickness of the reservoir zone, incorrect phase, or processing artifacts. Also the data were not prestack migrated so that may have had an impact on the dataset. Regardless, I felt that the AVO was quite successful.

Next, the inversions results backed the AVO results highlighting the channel zones. The P-impedance volume was quite accurate and I feel that it depicted the geology in the area. The anomalies (impedance lows) at the Colony level seemed to isolate the Colony reservoir zones adequately. The S-impedance highlighted the lithology contrasts on and off the channel. Although, the shear wave log values were hard to estimate due to the nature of the oil in the pore space and its associated Poisson’s ratio values (anywhere from 0.25 – 0.35), the use of the regional well with full waveform sonic data greatly improved the accuracy of the estimated shear wave values. This is quite an investigation in itself. I think that this is why not much LMR™ is done on oil reservoirs unless dipole sonic data are readily available. Not even the explorationists in this area seem to have a complete understanding for the shear response of the Colony. The problem with $\Lambda \cdot \rho$ is that oil is only slightly more compressible than water so differentiating between the two may be difficult, although the $\Lambda \cdot \rho$ volume had great anomalies at the well locations. The wells on the southwest end of the south channel didn’t show up as well but they are suspended so they may not represent an extensive oil pool. The $\mu \cdot \rho$ volume is simply the square of the S-impedance volume so I was expecting results as good as the $\Lambda \cdot \rho$ volume. As seen from the figures, the channel is quite very evident on the time slice with the south channel showing up better than the north one. The beauty of the LMR™ method is the integration between the $\Lambda \cdot \rho$ and $\mu \cdot \rho$ volumes to infer lithology and porefluid from seismic and well data.

The accuracy of the elastic impedance method is dependent on several factors. First, the input seismic data must have a sufficient angle distribution at the zone of interest. Also, the method requires sufficient well information, which should include V_p , V_s , and density. For the most accurate results measured shear sonic log information would be ideal; however in the absence of measured shear data, a good estimation should also give fairly accurate results. The elastic impedance method seems to predict hydrocarbon accumulations fairly accurately, as evidenced by good special correlation between elastic impedance lows and the producing well locations

on the 3-D survey. The far angle (33 to 44 degrees) seems to give more reliable results than the mid angle (21 to 32 degrees) as seen in Figures 27 and 28. This method gives similar results to the AVO/LMR™ analysis and may even produce a more localized analysis in terms of isolated zones. Because elastic impedance is a function of V_P , V_S , density, and incidence angle; distinguishing lithology based on the impedance volume itself may prove to be difficult.

In this paper AVO, LMR™, and elastic impedance methods were applied to a 3-D dataset on the Colony channel reservoir, with good success. The contrast in shear wave velocities in this area is quite different than other regions of the Western Canadian Sedimentary Basin and posed some difficulties with the LMR™ and elastic impedance portion of this exercise. This is an interesting problem and does not seem to be addressed in any literature on this exploration area.

ACKNOWLEDGEMENTS

I would like to acknowledge firstly Ken Hedlin and Art Chan of Husky Oil Operations Ltd. for providing me with this dataset to work on as well as some informative discussions, and secondly Geo-X Systems Ltd. for providing me the resources and time to work on this paper.

REFERENCES

- Allen, J. L. & Peddy C. P., 1993, 'Amplitude Variation with Offset: Gulf Coast Case Studies', SEG publication, Tulsa, Oklahoma.
- Connolly, P., Elastic Impedance, *The Leading Edge*, April 1999, Vol. 18, No. 4, p 438.
- Goodway et al., 1997, Improved AVO fluid detection and lithology discrimination using Lamé petrophysical parameters: " $\lambda\rho$ ", " $\mu\rho$ ", and " λ/μ fluid stack", from P- and S- inversions: CSEG Recorder, 3-5.
- Hedlin, K., 2000, 'Pore space modulus and extraction using AVO', SEG Expanded Abstracts.
- Putnam, P.E. and Oliver, T.A. 1980 Statigraphic traps in channel sandstones in the Upper Mannville (Albian) and east-central Alberta. *Bulletin of Canadian Petroleum Geology*, v.28, p. 489-508.
- Wrightman, D.M., Tilley, B.J., and Last, W.M., 1981, Statigraphic traps in channel sandstones in the Upper Mannville (Albian) and east-central Alberta: Discussion. *Bulletin of Canadian Petroleum Geology*, v.29, p. 622-629.
- Walker, R.G., and James N.P., 1992 Facies Models Response to Sea Level Change, GAC publication, p 136-137.
- Whitcombe, D., Connolly, P., Reagan, R., and Redshaw, T., Extended elastic impedance for fluid and lithology prediction, SEG 2000 Expanded Abstracts

Lambda-Mu-Rho™ and LMR™ are registered trademarks of PanCanadian Petroleum Ltd.